Structure of the Ca^{2+}/S100B/NDR Kinase Peptide Complex: Insights into S100 Target Specificity and Activation of the Kinase†

Shibani Bhattacharya,‡ Edward Large,‡ Claus W. Heizmann,§ Brian A. Hemmings,|| and Walter J. Chazin*,‡

Departments of Biochemistry and Physics, Center for Structural Biology, Vanderbilt University, Nashville, Tennessee 37232-8725, Department of Pediatrics, Division of Clinical Chemistry and Biochemistry, University of Zurich, Steinwiesstrasse 75, CH-8032 Zurich, Switzerland, and Friedrich Miescher-Institut, Maulbeerstrasse 66, CH-4058 Basel, Switzerland

Received June 25, 2003; Revised Manuscript Received October 1, 2003

ABSTRACT: NDR, a nuclear serine/threonine kinase, belongs to the subfamily of Dbf2 kinases that is critical to the morphology and proliferation of cells. The activity of NDR kinase is modulated in a Ca^{2+}/S100B-dependent manner by phosphorylation of Ser281 in the catalytic domain and Thr444 in the C-terminal regulatory domain. S100B, which is a member of the S100 subfamily of EF-hand proteins, binds to a basic/hydrophobic sequence at the junction of the N-terminal regulatory and catalytic domains (NDR_{62-87}). Unlike calmodulin-dependent kinases, regulation of NDR by S100B is not associated with direct autoinhibition of the active site, but rather involves a conformational change in the catalytic domain triggered by Ca^{2+}/S100B binding to the junction region. To gain further insight into the mechanism of activation of the kinase, studies have been carried out on Ca^{2+}/S100B in complex with the intact N-terminal regulatory domain, NDR_{1-87}. Multidimensional heteronuclear NMR analysis showed that the binding mode and stoichiometry of a peptide fragment of NDR (NDR_{62-87}) is the same as for the intact N-terminal regulatory domain. The solution structure of Ca^{2+}/S100B and NDR_{62-87} has been determined. One target molecule is found to associate with each subunit of the S100B dimer. The peptide adopts three turns of helix in the bound state, and the complex is stabilized by both hydrophobic and electrostatic interactions. These structural studies, in combination with available biochemical data, have been used to develop a model for calcium-induced activation of NDR kinase by S100B.

The cellular activity of EF-hand Ca^{2+} binding proteins is regulated by changes in calcium ion flux *in vivo*. The S100 subfamily has been implicated in Ca^{2+} homeostasis and a wide range of calcium-dependent signaling pathways that control cell growth and differentiation, cytoskeleton development, and cell surface receptor activities (*1*−*3*). Unlike the prototypical EF-hand calcium sensor calmodulin, S100 proteins exhibit tissue-specific expression and distinct intracellular localization, which restricts cellular targets but maintains the multifunctionality of the family. The differential regulation of S100 gene expression is an important clinical marker in a multitude of disease states such as cardiomyopathy (S100A1), psoriasis (S100A7), chronic inflammation (S100A8/A9), and several cancers (S100A2/A4/A6) (*4*).

S100B,[1] first isolated from nervous tissue glial cells, has been widely associated with the pathology of degenerative neurological disorders including Down syndrome, Alzheimer's disease, temporal lobe epilepsy, and brain damage after cardiac arrest (*4*−*7*). Functionally, S100B inhibits PKC-mediated phosphorylation and formation of microtubule assembly, stimulates enzyme activities, and regulates cell-cycle progression via interaction with transcription factors in the nucleus (*3*, *4*, *8*). When secreted into the extracellular space, S100B promotes neurite extension in concert with formation of a disulfide cross-linked state and is known to proliferate astrocytes by enhancing Ca^{2+} ion fluxes. S100B also exhibits cytokine-like activities through interactions with RAGE receptor (*9*−*11*). At sufficiently elevated levels of expression, S100B is toxic and has been shown to induce apoptosis of neurons (*4*). With over 20 known targets, S100B is the prototypical S100 protein.

One of S100B's targets is the nuclear serine/threonine kinase, NDR, a highly conserved and widely expressed member of the Dbf2 family of kinases that is critical in cell morphogenesis and proliferation (*12*, *13*). The physiological relevance of the interaction between S100B and NDR is evident from abnormal cytoskeleton development observed in glial cells when S100B expression is suppressed (*14*). In contrast, NDR kinase is hyperactive in melanoma-positive cells, which are clinically marked by S100B overexpression

† This research was supported by an operating grant from the NIH (R01 GM62112). Use of core facilities was supported in part by the Vanderbilt Center for Molecular Toxicology (NIH Grant P50 ES00267) and the Vanderbilt Ingram Cancer Center (NIH Grant P30 CA68485). C.W.H. was supported by the National Competence Center for Research (NCCR) on Neuronal Plasticity and Repair, the Wilhem Sander-Stiftung (FRG), and the Swiss National Science Foundation.

* To whom correspondence should be addressed. Phone: (615) 936-2210. Fax: (615) 936-2211. E-mail: walter.chazin@vanderbilt.edu.

‡ Vanderbilt University.

§ University of Zurich.

|| Friedrich Miescher-Institut.

[1] Abbreviations: PKA, protein kinase A; PKB, protein kinase B; HMQC, heteronuclear multiple-quantum coherence; HSQC, heteronuclear single-quantum coherence; NOE, nuclear Overhauser effect; TOCSY, total correlation spectroscopy; CaM, calmodulin; S100B, S100($\beta\beta$); NDR, nuclear Dbf2 related kinase; RMSD, root-mean-square standard deviation; RMD, restrained molecular dynamics.

10.1021/bi035089a CCC: $25.00
Published on Web 11/19/2003

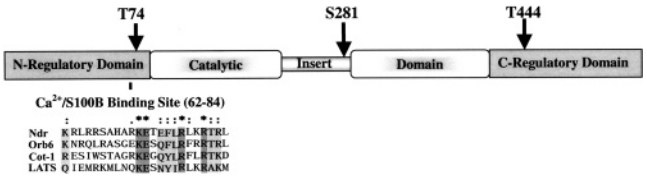

FIGURE 1: Schematic representation of the human NDR kinase structure. The catalytic domain contains 12 conserved structural motifs numbered according to a standard system of nomenclature used for eukaryotic kinases (*19*) (Supporting Information). N- and C-terminal regulatory domains flank the catalytic domain. Arrows indicate the three sites of phosphorylation in NDR. The Ca^{2+}/S100B binding site is conserved in the Dbf2 family of Ser/Thr kinases, which are involved in cell shape regulation and include NDR (*Homo sapiens*), Orb6 (*Schizosaccharomyces pombe*), Cot-1 (*Neurospora crassa*) and LATS (*Drosophila melanogaster*).

(*13*). The functional importance of Dbf2 kinases has been confirmed through gene mutational studies in other organisms (*15*−*17*). For example, yeast *Saccharomyces cerevisiae* Cbk1p mutants exhibit defects in cell shape, mating projection morphology, and cell separation (*18*).

The domain organization of the NDR/Dbf2 family of kinases (Figure 1) consists of a conserved catalytic domain (40−60% homology), which is flanked by N- and C-terminal regulatory domains of variable length and composition (see the sequence alignment in the Supporting Information). The sequence of the catalytic domain matches well to Ser/Thr and Tyr kinases (*19*). However, a unique feature of Dbf2 kinases is the presence of an insert of ~30 amino acids in the activation loop, which is required for nuclear localization (*12*) (Figure 1). At present, there are no representative structures of the Dbf2 kinase family.

The mechanism of NDR kinase activation has been proposed to involve phosphorylation at two conserved sites, Ser281 and Thr444, in a calcium-dependent manner, which in turn stimulates the catalytic domain to the "on" state prior to substrate binding (*20*, *21*). Recent data suggest that Ser281 in the activation loop is the primary site for autophosphorylation, a process that occurs in a Ca^{2+}/S100B-dependent manner (*21*). The phosphorylation of the second site Thr444, which is found in a conserved hydrophobic patch in the carboxy terminus, is carried out by an unknown upstream kinase. Interestingly, the phosphorylation of Thr444 is enhanced in the presence of calcium. It is unclear from existing studies if the unknown kinase is also a binding target for calcium-activated S100B or is part of an independent calcium-dependent pathway (*21*).

S100B has been shown to bind to a basic/hydrophobic cluster (NDR_{62-87}) at the junction of the N-terminal regulatory and kinase catalytic domains. This short segment is conserved in the Dbf2 family of kinases (Figure 1), suggesting it has similar structural and functional roles in the activation mechanism of the kinase. A single mutation in this junction region, NDR(Thr74 → Ala74), significantly impaired the kinase activity, suggesting a crucial structural role for this side chain in the interaction with S100B (*21*). Furthermore, deletion of the entire N-terminal regulatory domain eliminates S100B binding and also abolishes the kinase activity (*13*). This observation contrasts with CaM-dependent kinases, where deletion of the autoinhibitory segment contained within the C-terminal regulatory domain creates a constitutively active enzyme. Thus, the activation of NDR kinase must occur by a mechanism that is unlike that of CaM-dependent kinases (*21*, *22*). In this study, the structural details of the interaction between the N-terminal regulatory domain of NDR and Ca^{2+}/S100B have been characterized to gain insights into the mechanism of S100B regulation of NDR kinase activity.

S100 proteins constitute a unique class in the EF-hand calcium binding protein family with structures characterized by distinctive dimeric architecture and a noncanonical 14-residue Ca^{2+} binding loop in the N-terminal EF-hand (*23*). The three-dimensional structures of S100B have been determined in the apo and calcium-loaded states, as well as in complexes with the S100B binding regions of p53 and of the actin capping protein, CapZ (*24*−*28*). Activation by Ca^{2+} causes a shift in the position of helix III within each subunit of the dimer, which exposes a hydrophobic surface for binding to various target proteins (*23*). Comparison of the p53 and the CapZ fragments reveals differences in the orientation of the peptide with respect to S100B. In contrast, the S100A10/annexin II and S100A11/annexin I complexes are structurally alike (Cα rms deviation 0.87 Å), with respect to both peptide orientation and side-chain interactions, despite the differences in the annexin and the S100 protein sequences (*29*). Detailed comparative analyses of these complexes with the NDR kinase/S100B complex provide insight into the structural basis for S100 protein target variability and selectivity.

MATERIALS AND METHODS

Protein Expression and Purification. The gene for *Bos taurus* S100B (*30*) was subcloned into the pSV281 vector, a pET27 derivative with Kanamycin resistance, a His-tag, and an rTEV cleavage site. The resultant plasmid was transformed into *Escherichia coli* BL21 Codon plus (DE3) RIL competent cells (Stratagene), which were then overexpressed in isotopically enriched minimal media to get ^{13}C,^{15}N- and ^{15}N-labeled protein. The N-terminal polyhistidine-tagged ($MGSSH_6ENLYFQGA$) protein was purified on a Ni-NTA affinity column and yielded 10 mg/L pure protein suitable for further experiments. Since the tag was a random coil with no effect on peptide binding, it was not cleaved for NMR samples. The gene for the intact N-terminal regulatory domain of NDR kinase (NDR_{1-87}) from *H. sapiens* (*12*) was subcloned into pet3a vector and transformed into BL21(DE3) plys S cells that expressed into inclusion bodies in rich media. The protein was subsequently purified from inclusion bodies as described elsewhere (*31*).

NMR Samples. NMR samples of ^{1}H,^{15}N- and ^{1}H,^{13}C,^{15}N-enriched protein were made up in 20 mM d_{11}-Tris buffer (90% H_2O/10% D_2O) containing 5 mM $CaCl_2$, 30 mM KCl, and 10 mM d_{10}-DTT at pH 7.5. A ^{1}H,^{13}C,^{15}N-labeled sample was prepared in an identical buffer in 100% D_2O. The protein concentration determined by BSA analysis and UV absorbance at 280 nm was 1 mM in the S100B subunit. The HPLC-purified peptide (^{62}KRLRRSAHARKETEFLRLKRTRLGLE^{87}) was purchased from Genemed Synthesis Inc. (San Francisco, CA) and used without further purification. The purity was determined to be 99% by mass spectrometry, and the concentration was determined by amino acid analysis. A 1 M NDR_{62-87} peptide solution was made up in the above

specified buffer and titrated in 20−50 μL aliquots into the protein solution to achieve a final S100B subunit-to-peptide ratio of slightly greater than 1:1. The titration was judged to be complete on the basis of the absence of any chemical shift changes upon further addition of peptide. The final pH of the solution was adjusted to 7.5. An identical sample of ^{15}N,^{13}C-labeled S100B was prepared in the absence of a target peptide.

Chemical Shift and NOE Assignments of S100B. 3D experiments for protein resonance assignments were acquired on two different samples of the complex with ^{1}H,^{13}C,^{15}N-labeled S100B, one in H_2O and the other in D_2O. The spectra were recorded at 310 K on a Bruker 600 MHz *AVANCE* spectrometer equipped with a triple-axis-gradient probe. Sequential backbone assignments were made using 3D CBCA(CO)NH, 3D HNCA, 3D HN(CO)CA, and 3D HNCO experiments (*32*−*34*). Aliphatic side-chain proton and carbon assignments were made using 3D HCCH-TOCSY (15 ms of mixing) and 3D HCCH-COSY (*33*−*35*). For distance restraints and assignments ^{13}C-edited 3D NOESY-HSQC for aliphatic (*36*) and aromatic regions (*34*) of the spectra were acquired using H_2O and D_2O samples, respectively. A third sample of the complex containing ^{1}H,^{15}N-labeled protein was used to acquire ^{15}N-edited 3D NOESY-HSQC (*37*, *38*) and ^{15}N-edited 3D TOCSY-HSQC (52 ms of mixing) spectra on a Bruker 800 MHz *AVANCE* spectrometer. The mixing time used for all NOESY spectra was set to 100 ms.

The backbone resonances of 87 of the 91 residues in the S100B/NDR$_{62-87}$ complex were assigned. Due to chemical exchange on the intermediate time scale, residues Gly22, Asp23, and Lys24 in the first Ca^{2+} binding loop and Gln50 in the linker region were not observed. A total of 97% of the side-chain chemical shifts were assigned. All chemical shifts have been deposited under BMRB accession code 5838. The NOEs observed in the complex of S100B with NDR$_{62-87}$ were identified in several phases. The NOEs within S100B subunits were assigned through the analysis of 3D ^{13}C- and ^{15}N-edited NOESY-HSQC spectra. The NOEs across the dimer interface were identified in the same spectra since the many published structures of S100B all show identical arrangements of the two subunits (*26*−*28*, *39*−*41*). On the basis of this initial assumption, 57 intersubunit NOEs were uniquely identified. In addition, 16 NOEs could be assigned to both intra- and intersubunit correlations, and these were included in the calculations but with the highest upper bounds. Identification of NOEs between the protein and the peptide involved both 2D and 3D J-filtered experiments described below (*42*, *43*).

NDR$_{62-87}$ Peptide Assignments. To facilitate the chemical shift assignments of the bound peptide, the free peptide was assigned first and the chemical shift changes were mapped as S100B was titrated in to achieve 2:2 stoichiometry in the final complex. The following experiments were acquired on a 600 MHz spectrometer equipped with a ^{1}H−{^{13}C,^{15}N} triple-resonance CryoProbe (Bruker) with single-axis *Z*-gradient (*42*, *44*, *45*): 2D ^{15}N F2-filtered NOESY on a sample containing ^{1}H,^{15}N-labeled protein, 2D ^{15}N,^{13}C F2-filtered NOESY and 2D ^{15}N,^{13}C F2-filtered TOCSY (40 ms of mixing) on a sample containing ^{1}H,^{13}C,^{15}N-labeled protein, and 3D ^{13}C F1-edited ^{13}C,^{15}N F2-filtered HMQC-NOESY (*43*). The latter sample was also used to acquire a 2D ^{15}N,^{13}C F1/F2-filtered NOESY spectrum and a 2D ^{15}N,^{13}C F1/F2-filtered COSY spectrum on the 800 MHz spectrometer. Homonuclear 2D NOESY, TOCSY, COSY spectra were acquired for the free peptide sample at 310 K on the 800 MHz spectrometer. Complete backbone and partial side-chain assignments were obtained for peptide residues NDR$_{64-86}$. All data sets were processed and analyzed in Felix-2000 with standard parameters described elsewhere (*33*). 2D and 3D NOESY cross-peak assignments were facilitated by the use of the SANE software package for structure-assisted distance filtering (*46*).

Distance and Angle Restraints. Input distance constraints for the protein were generated from NOESY cross-peak intensities with the upper bounds set to 3.5, 4.5, and 6.0 Å in the initial round of calculation. Any distance constraint assigned, but whose intensity could not be accurately determined, was assigned an upper bound of 6.0 Å. The upper bounds were subsequently fine-tuned in the later stages of the calculation, with the final value set to 3.5, 3.7, 4.5, and 6.0 Å for intensities measured in the 3D ^{15}N-edited NOESY-HSQC spectrum and 3.5, 4.0, 4.5, and 6.0 Å for intensities derived from the 3D ^{13}C-edited NOESY-HSQC spectrum. Distance restraints between protons in the peptide, and between the protein and the peptide, were also generated from cross-peak intensities with the same upper bounds. Pseudoatom distance corrections were added where necessary (*47*). To improve the accuracy of the structure, a loose upper distance bound of 8.5 Å was used for protein−peptide NOEs, without any further corrections added for pseudoatoms. Stereospecific assignments were made for the protein based on the basis of NOEs in the GLOMSA module within the DYANA suite of programs (*48*, *49*). Restraints on torsion angles ϕ and ψ were calculated using Hα, C′, Cα, Cβ, and N chemical shifts in the program TALOS (*50*). For the NDR peptide, Hα shifts were used to calculate the dihedral angle restraints in TALOS. Only those angles in the helical region of the Ramachandran plot, which were supported by the observation of i to $i + 3/i + 4$ NOEs, were used in the final calculations (NDR$_{72-86}$). To ensure the data were not overinterpreted, the range used for dihedral angles was set to twice the value predicted by TALOS.

Structure Calculations. An initial set of 50 S100B subunit structures was calculated with 15 restraints/residues using the program DYANA (version 1.5) (*49*) and provided an ensemble with a mean target function value of 0.38 ± 0.69 and no distance violations greater than 0.2 Å or angle violations greater than 2°. This was followed by 1000 steps of energy minimization prior to a 20 ps restrained simulated annealing run in a vacuum using AMBER (version 7.0) (*51*, *52*). A set of 50 peptide structures were calculated and refined in a similar manner using intrapeptide restraints (six per residue). Dimer structures were produced starting with the two best subunit structures. Each starting structure was duplicated, and the two molecules were oriented and placed 80 Å apart using NAB (*53*). The two subunits were docked with 73 × 2 restraints over 20 ps and refined for an additional 20 ps using restrained MD simulations in AMBER (version 7.0) (*54*, *55*). This process was repeated 33 times with the second molecule in a different relative orientation each time, producing an ensemble of 66 dimer structures.

The final ensemble of structures of the complex were generated by selecting the four best dimer structures and docking two copies of the best peptide structure into the two

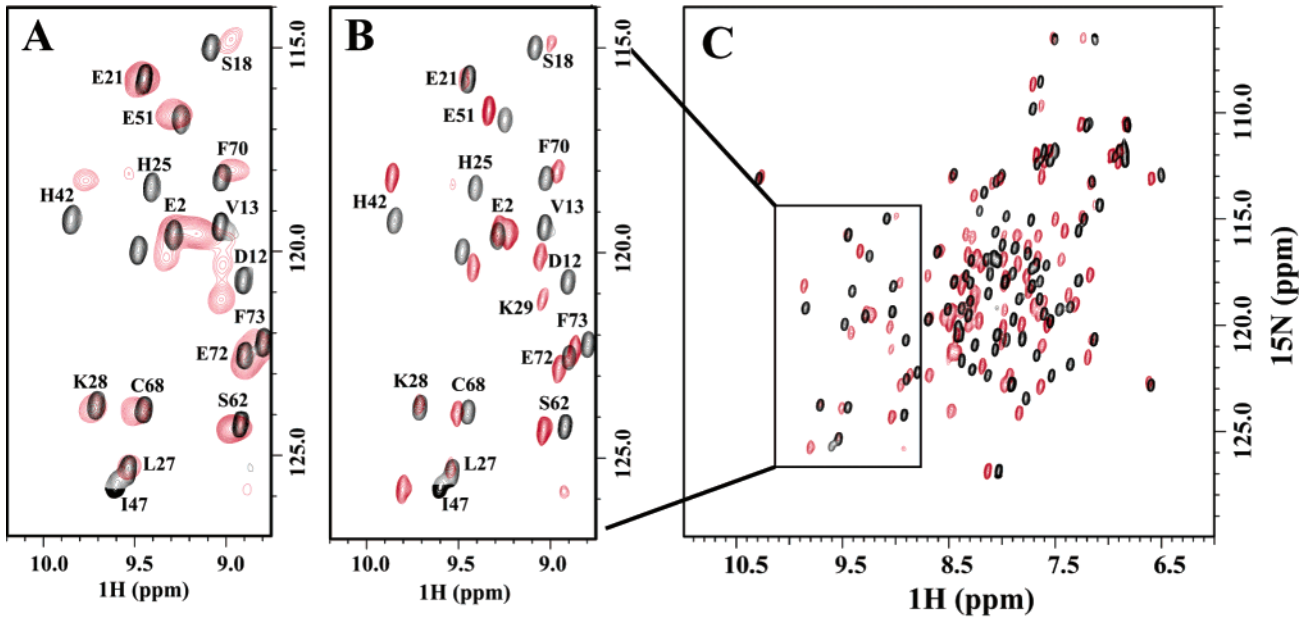

FIGURE 2: Effect of NDR binding on the $^1H-^{15}N$ HSQC spectra of Ca^{2+}/S100B. Selected regions of the spectrum with (A) NDR_{1-87} bound and (B) NDR_{62-87} are shown in the two panels. Black contour lines are used for Ca^{2+}/S100B and red contour lines for the complexes. (C) Complete spectrum of the reference Ca^{2+}/S100B state (black) superimposed on the Ca^{2+}/S100B/NDR_{62-87} complex (red).

binding sites of the S100B dimer. To ensure convergence, the two peptides were placed symmetrically in 32 different orientations at a distance of 20 Å from the center of the dimer interface using NAB. During the 20 ps RMD docking, the peptide−protein distance restraints (39 × 2) were ramped from 0 to 32 kcal mol^{-1} $Å^{-2}$ and all intrapeptide and intraprotein distance restraints maintained during the simulation with a 32 kcal mol^{-1} $Å^{-2}$ force constant (*54*, *55*). The resultant 32 × 4 structures of the ternary complex were subjected to two rounds of 20 ps simulated annealing runs.

The program FindFam (*56*) was used to determine that 20 structures were adequate to represent the final ensemble. The family of 20 best structures was selected on the basis of the smallest restraint violation energies and favorable total molecular energies. The structures were analyzed with Procheck-NMR software (*57*). A total of 98% of the residues reside in the favored regions of the Ramachandran plot, with the exception being Asp23, Lys24, and Asp61 in the calcium binding loops and Lys48 in the peptide binding linker region. The coordinates of the structure have been deposited with the Protein Data Bank (1PSB). The program Interhlx was used to calculate the interhelical angles (K. Yap, University of Toronto). The representations of the molecular structures in the figures were created in the program MOLMOL (*58*) and Insight II (Accelrys Inc.).

RESULTS

The N-terminal regulatory domain of NDR kinase (residues 1−87), which contains the putative S100B binding site (residues 62−87), is predicted to have helical propensity, but the tertiary fold could not be homology modeled owing to the uniqueness of the sequence. Attempts to overexpress and purify NDR_{1-87} in *E. coli* yielded protein that did not form a well-folded globular structure and was characterized by low solubility at neutral pH. Despite these difficulties, sufficient quantities of the domain were produced for preparing NMR samples of S100B/NDR_{1-87} at <100 μM concentrations. The use of a CryoProbe (Bruker) provided a sufficient signal-to-noise (S/N) ratio to compare the NMR spectrum with that of the complex of S100B with the NDR_{62-87} peptide. The corresponding overlay of the $^1H-^{15}N$ HSQC spectra of S100B shows that they are nearly identical (Figure 2). The small differences in the spectra arise mainly from small differences in the S100B:NDR ratio as well as the broader lines for the complex with NDR_{1-87}, whose mass is greater by a factor of 1.5. The presence of only one set of signals for the S100B homodimer in both complexes indicates that two molecules of NDR_{1-87} bind symmetrically to the two subunits of Ca^{2+}/S100B. Given that the stoichiometry of the complex and the mode of binding to S100B are the same for the intact N-terminal regulatory domain and the peptide, the smaller complex of S100B with NDR_{62-87} could be used for the purpose of structure determination.

Structure of the S100B/NDR_{62-87} Complex. Complete ^1H, ^{13}C, and ^{15}N chemical shift assignments were made using the standard heteronuclear strategy (*33*). This enabled the location of the NDR_{62-87} peptide binding site on S100B to be determined on the basis of changes in S100B amide proton chemical shifts (Figure 3A). A significant difference (>0.1 ppm) in amide proton (^1H) resonances was observed for residues in helix I (Asp9, Ile11, Asp12, Val13, Phe14), the linker (Ser41, His42, Phe43, Leu44, Glu45, Glu46, Ile47), helix III (Glu51, Val52, Val53, Val56), and helix IV (Ala78, Thr82, Cys84, Glu86, Phe88). Plotting these differences as a function of varying peptide ratio (Figure 3B) yields an average binding constant of 20 ± 10 μM and 2:2 stoichiometry for the complex.

Constraints for the structure of the complex of S100B and NDR_{62-87} were generated by standard methods. The critical intermolecular NOEs were identified in a series of 2D and 3D filtered and filter-edited NOESY spectra (Figure 4). Table 1 summarizes the restraints used in each category for the different stages of calculation. Since no experimental con-

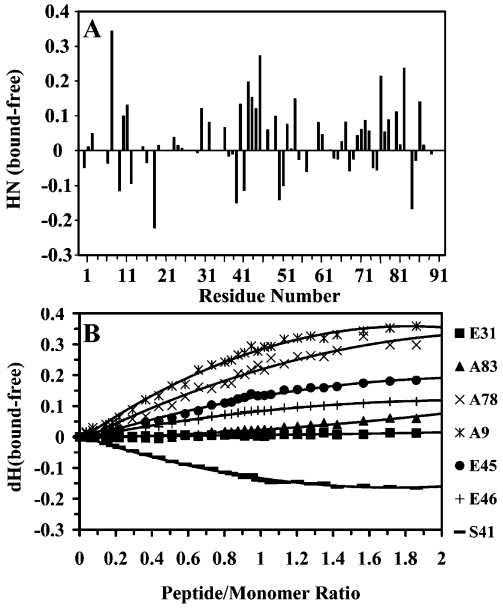

FIGURE 3: Changes in S100B chemical shifts upon binding NDR. (A) Amide proton chemical shift differences plotted against the protein sequence. (B) Chemical shift differences as a function of peptide:monomer ratio for select backbone resonances.

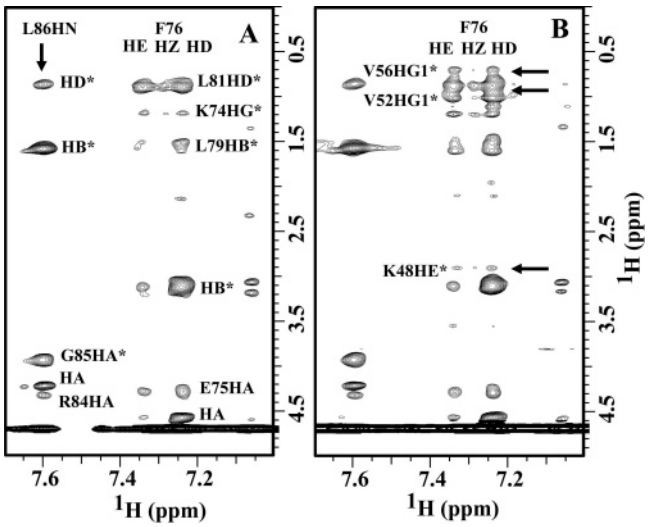

FIGURE 4: Analysis of proton−proton contacts of the unlabeled NDR_{62-87} peptide. (A) Portion of a 2D $^{13}C,^{15}N$ F1/F2-filtered NOESY spectrum of the complex. Intrapeptide NOE correlations observed between side-chain protons of NDR (F76) and the amide protons of NDR (L86). (B) Portion of a 2D $^{13}C,^{15}N$ F2-filtered NOESY spectrum of the complex showing additional correlations between side-chain protons of NDR (F76) and those of S100B side chains. Degenerate protons are marked with asterisks.

straints were determined for the Ca^{2+} ions, the structure calculations were done in vacuo without ions. The 2:2 stoichiometry of the complex presented some challenges for structure determination in AMBER and involved two docking steps, starting with the generation of separate families of subunit and peptide structures, respectively (described in the Materials and Methods). The family of 20 conformers representing the solution structure of the complex is shown in Figure 5A. Table 1 contains a summary of structural statistics for the ensemble, which exhibits no distance violations greater than 0.2 Å, no torsion angle violations greater than 5°, and large negative molecular energies.

In the structure of the complex, helix I (0.24 Å) and helix II (0.14 Å) of the N-terminal EF-hand and helix III (0.19 Å) of the C-terminal EF-hand are very well determined, but helix IV (0.35 Å) is less well defined because it is frayed at its C-terminus (Table 1). Also, the N-terminal Ca^{2+} binding loop is less well defined than the C-terminal binding loop. Although the linker between the two EF-hands does not have any regular secondary structure, it is not completely disordered, the result of long-range contacts between residues Phe43 and Leu44 and residues in helix III (Ile36) and helix IV (Phe76, Ile80, Cys84). The backbone RMSD of the family of structures of the entire complex (0.78) is higher than that of the dimer alone (0.60), reflecting the higher uncertainty both of the peptide backbone and of its location with respect to the protein subunit because it is not as well constrained by experimental data as the protein.

NDR_{62-87} is unstructured at its N-terminus (residues 62−71) and adopts a helical conformation from Lys72 to Leu86. The C-terminal end of the peptide is constrained by interactions with NDR (Leu86) and Phe87 near the C-terminus of helix IV of S100B (Figure 5B). The N-terminal end of the NDR helix is anchored by several hydrophobic contacts between the aromatic ring of NDR (Phe76) and side-chain methyl groups from Ile47, Val52, and Val56 of S100B (Figure 5B). The side chains of NDR (Leu78, Leu79, Lys80, Arg83) also make several contacts within the hydrophobic core of S100B (Figure 5B).

A significant number of electrostatic interactions are found in the majority of structures in the ensemble (Figure 5C). These involve side chains from the helical region of NDR_{62-87} (Lys72, Glu73, Arg78) and the linker region of S100B (Glu45, Glu49, Glu51, Lys55). Our structure shows that NDR_{62-87} does not form an ideal amphipathic helix in the complex. Instead, the interface is composed of a mixture of positively charged and hydrophobic residues. Similar observations have been made in structures of other S100/target complexes, as well as for certain calmodulin/target complexes.

Comparison to Other S100 Protein/Target Complexes. Like calmodulin, multiple binding modes have been observed for various S100-activated targets, despite the sequence and structural similarities of their largely hydrophobic binding sites. Figure 6 shows protein surfaces and peptide orientations for six different S100 protein/target peptide complexes. While there appear to be similar arrangements for some of the peptides, detailed inspection shows that each of the complexes has distinct structural characteristics. It is intriguing that even the four complexes of S100B are so different from each other. The theme of variation is perhaps most evident in the two structures of the TRTK-12 peptide bound to rat and human S100B. In the complex with human S100B, the peptide adopts a random coil conformation, making multiple contacts with helix III and helix IV (Figure 6C). In contrast, the peptide adopts a single helical turn and lies parallel to helix IV in the rat S100B complex (Figure 6F). The dramatic difference between the two S100B structures with the TRTK-12 peptide is intriguing since the protein sequence differs at only two positions: 62 in the calcium binding loop (Glu in rats vs Asn in humans) and 78 in helix IV (Ser in rats vs Ala in humans). Thus, the origin of this discrepancy is not evident. It would be of interest to measure NMR residual

Table 1: Structural Statistics for the S100B/NDR Complex

Constraints (3274)					
	S100B (per subunit)	NDR_{62-87}		S100B (per subunit)	NDR_{62-87}
intramolecular			intramolecular		
intraresidue	541	89	long-range	174	
sequential	298	23	ϕ/ψ	155	28
medium-range	205	12	intermolecular	73	39

Precision (RMSD)			
	residues	backbone (Å)	heavy atoms (Å)
complex	(2−89, 74−85)[a]	0.78	1.32
dimer	(2−89)	0.60	1.10
subunit	(2−89)	0.49	1.05
helix I	(2−20)	0.24	0.92
helix II	(29−39)	0.14	0.67
helix III	(50−60)	0.19	0.81
helix IV	(70−89)	0.35	0.99
Ca^{2+} binding loop I	(21−28)	0.42	1.10
Ca^{2+} binding loop II	(61−69)	0.22	0.77
linker	(40−49)	0.38	1.06
peptide	(74−85)	0.51	1.05

Agreement with Constraints					
⟨distance⟩ (Å)		⟨angle⟩ (deg)		⟨energy⟩ (kcal mol^{-1})	
0.1 Å < d < 0.2 Å	4.5	θ < 5°	10.6	$E_{constraint}$	13.6 ± 0.8
0.2 Å < d	0.0	θ > 5°	0.0	E_{AMBER}	−3384 ± 41
d_{max}	0.14	t_{max}	4.4	$E_{Lennard-Jones}$	−1400 ± 17

[a] Peptide residues included in the RMSD calculations.

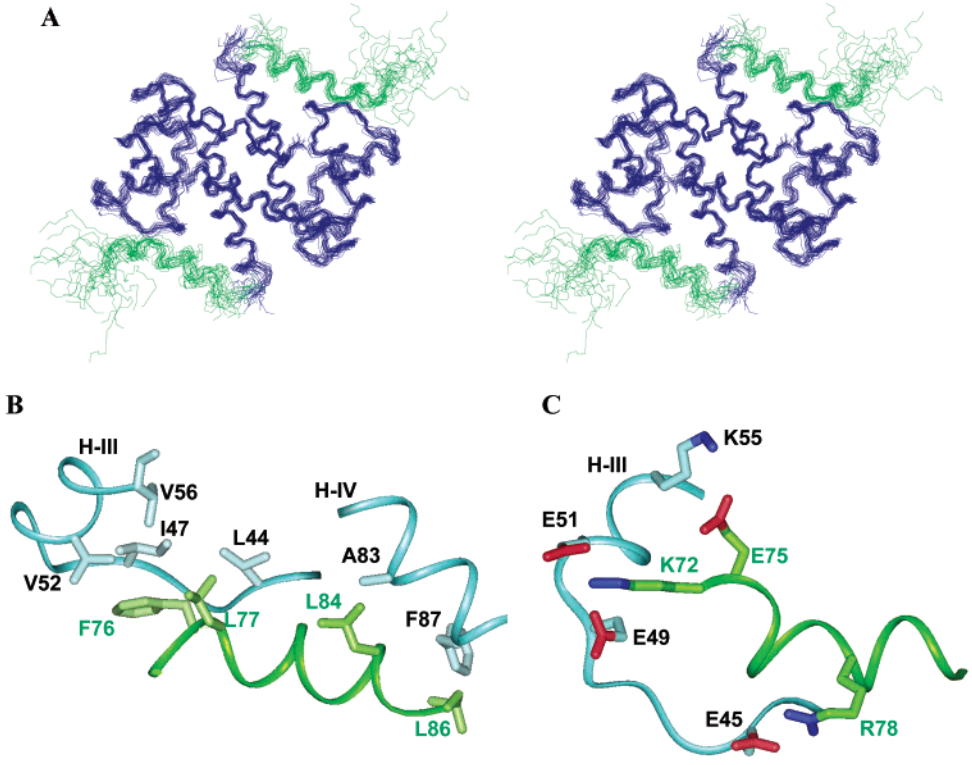

FIGURE 5: Structure of the Ca^{2+}/S100B/NDR_{62-87} complex. (A) Stereoview of the ensemble of 20 representative conformers. The protein is cyan and the peptide green. (B) Hydrophobic contacts between S100B and the NDR peptide. (C) Electrostatic complementarity between S100B and NDR_{62-87}. Residues from the protein are labeled in black and those from the peptide in green. The charged functional groups in side chains in panel C are colored red (−) and blue (+).

dipolar couplings to ensure the TRTK-12 peptide is accurately oriented with respect to the protein.

The observation of alternate peptide binding modes leads to questions about the extent of calcium-induced opening of the EF-hands required for holding different targets within the binding site. Clearly, the apo state conformation of S100 proteins is distinct from the Ca^{2+}-loaded state conformation (cf. interhelical angles in Table 2). In contrast, there seem to be much smaller differences in interhelical angles between the Ca^{2+}- and target-bound states (*29*, *39*, *40*). The sole

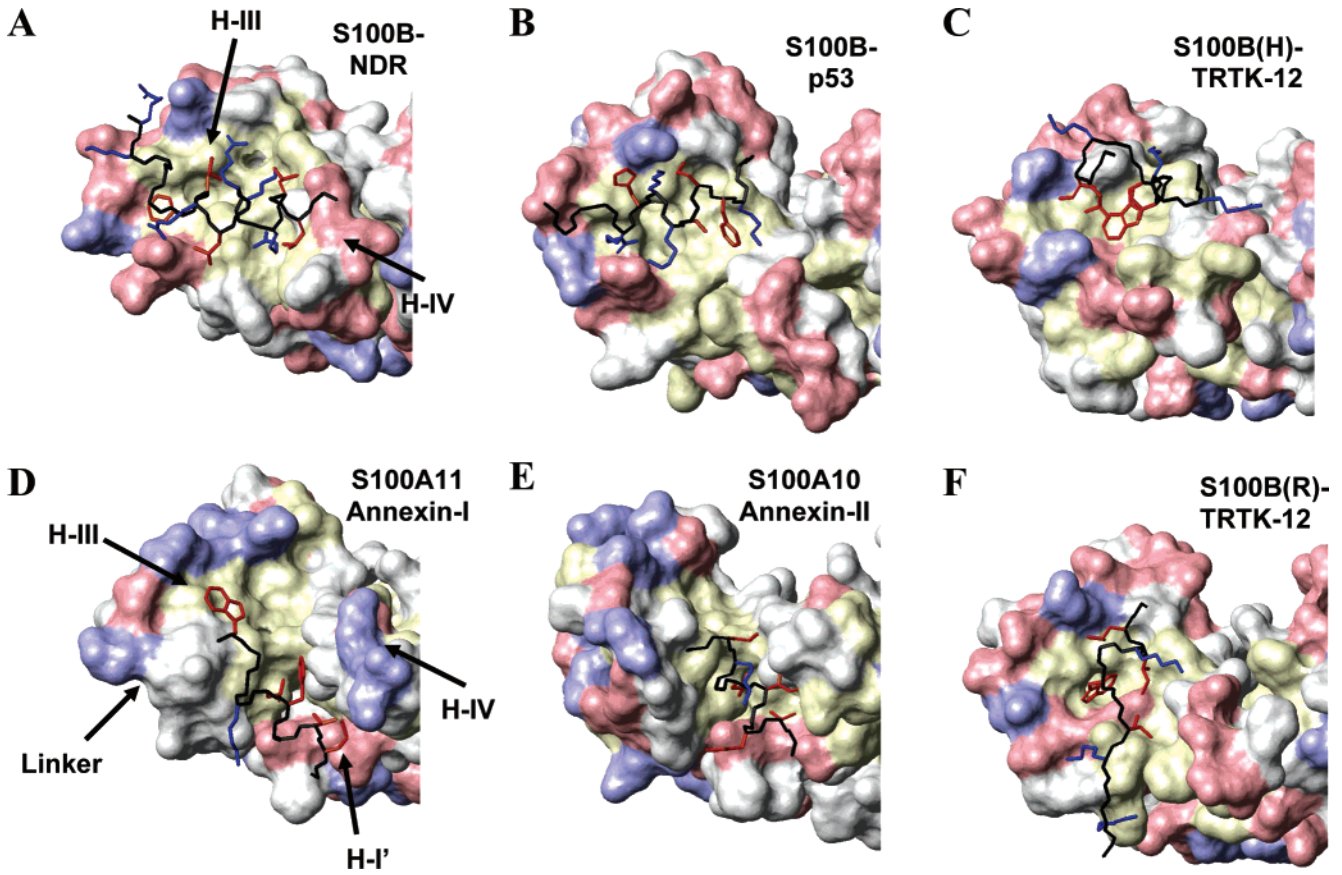

FIGURE 6: Comparison of S100 protein target peptide binding modes. (A) S100B/NDR$_{62-87}$ peptide complex, 1PSB. (B) S100B/p53$_{367-388}$ peptide, 1DT7. (C) S100B (human)/TRTK-12, 1MQ1. (D) S100A11/annexin I (residues 1−11) N-terminus peptide, 1QLS. (E) S100A10/annexin II (residues 1−10) N-terminus peptide, 1BT6. (F) S100B (rat)/TRTK-12, 1MWN. The protein surface representation was generated within MOLMOL (*58*) using different colors to display the properties of the binding surface (yellow for hydrophobic, red for acidic, blue for basic).

Table 2: Interhelical Angle Comparisons of S100 Structures[a]

	PDB code	H I/II	H I/III	H I/IV	H II/III	H II/IV	H III/IV
apo-S100B (a)	1CFP	134 ± 4	−64 ± 4	114 ± 3	145 ± 4	−44 ± 4	169 ± 5
Ca^{2+}/S100B (b)	1MHO	138	−122	132	100	−30	101
Ca^{2+}/S100B/Ndr$_{62-87}$ (b)	1PSB	141 ± 3	−119 ± 3	135 ± 2	101 ± 3	−25 ± 2	100 ± 3
Ca^{2+}/S100B (c)	1QLK	133 ± 5	−122 ± 6	127 ± 3	105 ± 4	−38 ± 4	101 ± 4
Ca^{2+}/S100B/p53 (d)	1DT7	120 ± 3	−126 ± 2	124 ± 1	113 ± 2	−28 ± 2	107 ± 2
S100A10 (e)	1A4P	134 ± 1	−106 ± 4	130 ± 1	119 ± 3	−30 ± 1	117 ± 1
S100A10/annexin II (f)	1BT6	136 ± 1	−106 ± 2	131 ± 1	118 ± 2	−33 ± 1	113 ± 2

[a] The range of residues used to define the helices in the different structures were as follows: (a) bovine apo-S100B, H I (3−19), H II (29−37), H III (50−60), H IV (70−83); (b) bovine Ca^{2+}/S100B, H I (2−20), H II (29−39), H III (50−60), H IV (70−89); rat Ca^{2+}/S100B, H I (3−19), H II (29−39), H III (50−60), H IV (70−83); rat Ca^{2+}/S100B/p53, H I (3−19), H II (29−39), H III (50−60), H IV (70−88); human S100A10, H I (2−17), H II (29−39), H III (50−60), H IV (70−84); human S100A10/annexin II, H I (3−19), H II (27−37), H III (50−58), H IV (68−89).

exception is that of S100A10, which is constitutively bound to its target and does not require Ca^{2+}-dependent opening of the apo structure (*59*). The apparent lack of change in helix orientations of the two EF-hands suggests that the hydrophobic binding pocket does not undergo large-scale conformational changes in the presence of the target; i.e., the gross features are preformed by Ca^{2+} loading. In contrast, reorganization of side chains is extensive and leads to optimization of specific sets of intermolecular contacts and formation of stable complexes.

Examination of the S100 protein sequence alignment in regions important for target binding for the complexes shown in Figure 6 provides further insight into the variability of side-chain contacts. The location of several hydrophobic contacts involving residues from helix III, the linker, and helix IV are conserved in S100/target complexes (Figure 7). For instance, a series of hydrophobic contacts in S100B involve Val52, Lys55, and Val56 in helix III and complementary residues from different targets [NDR (Phe76), p53 (His380), and TRTK-12 (Trp7)]. In the S100A11/annexin I complex, Trp11 from the annexin peptide interacts with corresponding residues Val57 and Met61 in helix III of S100A11. The aromatic ring in the target appears to serve as an anchor point for binding, and differences in this anchor side chain are anticipated to have significant impact on the binding affinity. In fact, among the various S100B complexes, the K_d ranges from ~10 μM for the small His380 in

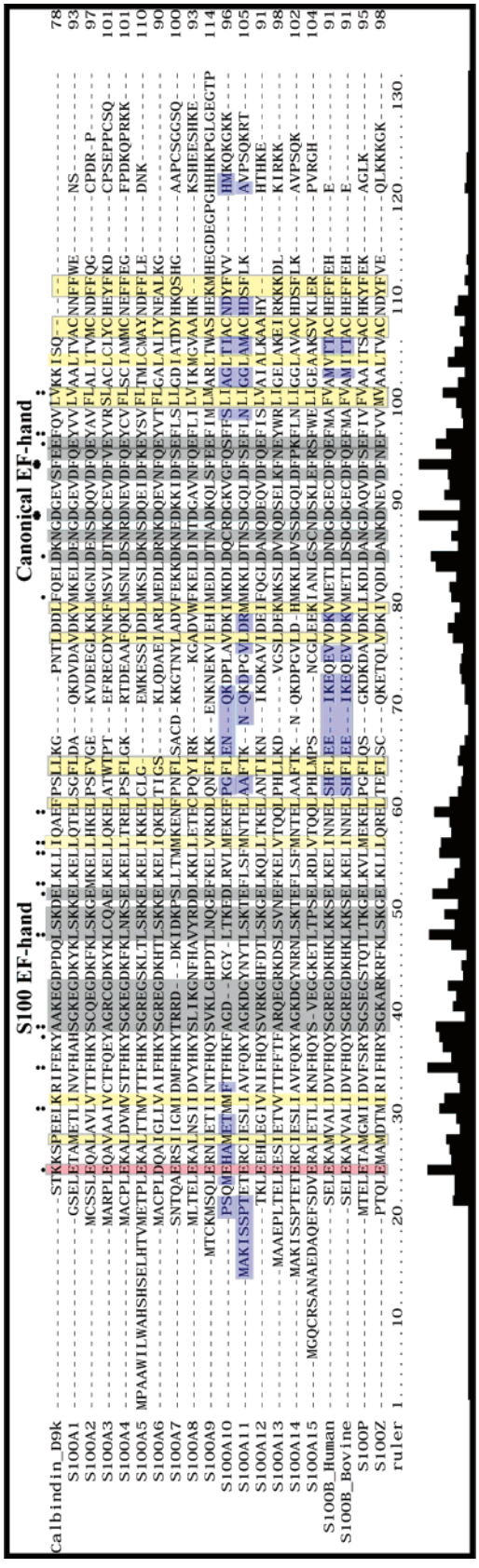

FIGURE 7: Human S100 protein sequence alignment in ClustalX (*76*). The gray regions represent the conserved calcium binding loops. Structurally conserved hydrophobic residues important for binding the target peptide are indicated in yellow. Binding sites that show lower sequence homology in the linker and helix IV are indicated in blue for S100A10/S100A11 and S100B.

p53 to ~0.3 μM for the much larger Trp7 in the TRTK-12 complex.

In S100B, a second critical target binding pocket is formed by Ala83, Cys84, Phe87, and Phe88 in helix IV, which contact structurally homologous residues in NDR (Leu86), p53 (Phe385), and TRTK-12 (Ile9). This C-terminal hydrophobic patch is conserved in S100A11 (Ala88, Cys89, Phe93) and interacts with Phe6 in the annexin I peptide. The importance of this contact point is consistent with mutational studies showing that S100 residues at the very C-terminus of helix IV, Glu86−Glu91 in S100B (*60*), Phe88−Ser93 in S100A1 (*61, 62*), Asp91−Ile94 in S100A11 (*63*), and Gly97−Pro114 in S100A9 (*64*), are critical for target binding. Interestingly, the unique ancestral S100 protein calbindin D_{9k} lacks this hydrophobic patch at the C-terminus of helix IV. This observation is consistent with the absence of Ca^{2+}-dependent targets for calbindin D_{9k} and its apparent function in Ca^{2+} homeostasis as opposed to Ca^{2+} sensing (*65*) (Figure 7).

In addition to hydrophobic interactions, there are also important charge−charge interactions contributing significantly to the stability of S100/target complexes. Many of these originate from residues in the linker between the two EF-hands, which contains the least sequence conservation among S100 proteins. Examples include interactions involving S100B residues Glu45 and Glu46 with NDR (Arg78) or p53 (Arg379), as well as S100B Glu46 with TRTK-12 (Lys4) (Figure 5). A segment of acidic residues, ^{45}EEIKEQE^{51}, at the junction of the linker and helix III of S100B also has an effect on determining the orientations of $p53_{367-388}$ and NDR_{62-87}, which both contain a basic patch near their N-termini (*41*). Note there is no analogue for these contacts in the S100A10/A11 structures (Figure 6).

Unlike calmodulin, S100 target sequences cannot be classified on the basis of separation of hydrophobic anchor points, as there is large variation in the content and position of the key basic/hydrophobic residues (Table 3). For example, the putative consensus sequence "+OXO*XOO" (+ = basic, O = hydrophobic, * = hydrophilic, X = variable) for S100B targets, which is contained in the TRTK-12 peptide, shows no homology to p53, NDR, or the annexin N-terminal peptides (*66*, *67*). This in turn emphasizes the critical importance of the variation in hydrophobic and charged side chains for generating the variations in the S100 protein binding surface needed for recognizing such a diverse range of targets.

DISCUSSION

Structural and sequence comparisons show that S100 proteins have similar patterns of hydrophobic residues, which provide an overall similarity in their binding surfaces (Figures 6 and 7). The selectivity for different targets is created in part by side chains in these conserved hydrophobic patches as well as differences in the less conserved regions of S100 proteins. In this view, the conserved but not identical hydrophobic sites in helix III and helix IV serve to capture the target and confer an intrinsic binding affinity. The differences in the bulk of these hydrophobic side chains clearly influence the topology of the binding surface and hence the overall shape complementarity between the S100 protein and target (Figure 6). For example, although helix

Table 3: Comparison of Peptide Sequences

S100 protein	PDB code	target peptide	peptide sequence[a]
S100B	1PSB	NDR (62−87)	KRLRRSAHAR*KE*TE*F*L*RLK*RT*R*LG*L*E
S100B	1DT7	P53 (367−388)	SHLKSKKG*Q*STS*RH*KK*LMFKTE*
S100B	1MWN	TRTK-12	TRT*KI*D*W*N*KIL*S
S100B	1MQ1	TRTK-12	TRTKIDWNKILS
S100A10	1BT6	annexin II (1−10)	T*VH*EI*LS*K*LS*
S100A11	1QLS	annexin I (1−11)	AMV*S*A*FLK*Q*AW*

[a] Peptide residues that make contacts with the protein (interatomic distance less than 5 Å) are italicized.

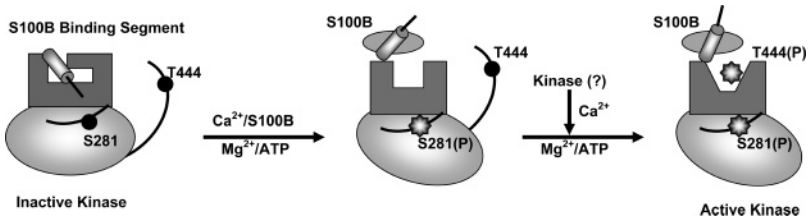

FIGURE 8: Schematic representation of the kinase activation mechanism indicating the key steps starting with Ca^{2+}/S100B-induced release of autoinhibitory interactions in the N-lobe of the catalytic domain. This enables autophosphorylation of Ser281 in the activation loop and transphosphorylation of Thr444 in the C-terminal regulatory domain by an independent Ca^{2+}-triggered pathway (*21*). Ser281(P) and Thr444-(P) through intramolecular interactions induce conformational changes in the active site and N-lobe structure, respectively and this activates the kinase fully.

III/IV interhelical angles are not significantly different, the hydrophobic binding pocket of S100B appears much wider than in S100A10 or S100A11.

The charge complementarity between the protein and target involving interactions from the linker and helix III also play a role. But in contrast to the conserved hydrophobic patches, these sites vary in both content and location in the 3D structure over the S100 family (Figure 7). Overall, the additive effect of these multiple differences helps to generate the target and functional specificity of different S100 proteins. By way of example, consider that the residues in S100B that directly contact NDR are 38% identical to corresponding residues in S100A2, 34% identical to those in S100A4, and 15% identical to those in S100A6. Yet despite these very significant sequence identities, all tested negative for inducing NDR activity. Even S100A1, which has 54% identity to S100B among the residues that contact NDR, activates the kinase only very weakly. One must conclude that the sequence differences at critical locations in the binding site clearly limit the ability to form a stable functional complex.

The driving force for S100 target binding in a particular orientation and with specific secondary structure content is derived from a complex interplay of forces. These forces include burying a significant part of the peptide through favorable hydrophobic side-chain contacts, electrostatic interactions, entropic consequences of the disorder-to-order transition, and resultant desolvation effects (*68*). Energetically, the conformational changes in the target are tightly coupled to those of the S100 protein (*39*, *40*, *69*), and like calmodulin/target complexes, it is known to modulate the calcium sensor properties (*70*, *71*). Therefore, the ability to bind a specific target with adequate affinity is crucial for synchronizing the Ca^{2+}-signaling pathways with the calcium ion flux in different activation stages of the cell.

Implications for the Kinase Activation Mechanism. The interactions of S100B with the intact N-terminal regulatory domain of NDR indicate a unique activation mechanism that does not involve a "pseudosubstrate" blocking the active site (*13*, *74*). To extend our structural analysis of possible roles for S100B in the activation of NDR, a homology model of the catalytic domain was constructed using PKA in the substrate-bound state as a structural template (Supporting Information) (*77*). The resultant model of the NDR catalytic domain revealed a bilobe structure that encloses the active site cleft, similar to other Ser/Thr kinases from the AGC family (Figure 8) (*75*). This structural model of the NDR catalytic domain shows that the access of the helical S100B binding segment to the active site is impeded. However, this segment can directly interact with residues from a complementary charged/hydrophobic patch within the N-lobe. Such a structural arrangement would be reminiscent of EphB2, a receptor tyrosine kinase (*82*). The structure of the inactive EphB2 kinase reveals intramolecular interactions involving an N-terminal juxtamembrane segment and the N-lobe of the catalytic domain, which blocks access to the ATP binding loop and induces a kink in the αC helix. In the EphB2 kinase, the first step of activation involves phosphorylation of a Tyr in the N-terminal segment, which eases the structural distortions.

The EphB2 kinase family and recently published biochemical data from Tamaskovic et al. (*21*) support a model for the activation mechanism of NDR where binding of S100B releases inhibitory N-lobe interactions, which in turn enables ATP to bind and initiate the autophosphorylation of Ser281 (Figure 8). These events lead to favorable alignment of the active site residues for substrate binding, as has been shown in the closely related PKA kinases (*78*, *79*). The next step would involve Ca^{2+}-dependent phosphorylation of Thr444 by an upstream kinase (*21*). The recent structure of PKB/Akt suggests (*81*) that interactions between the phosphorylated Thr444 and the N-lobe promote additional structural changes that complete the activation mechanism of the kinase.

This simplified view of the N-terminal regulatory domain function leads to two important questions regarding the extent to which this domain is dissociated from the catalytic domain when bound to S100B and the role of a second binding site

on S100B. Since deleting the N-terminal regulatory domain reduces the activity of the kinase, the importance of bound S100B is not just limited to relieving autoinhibitory interactions and requires further investigation. Such studies would also be relevant to understanding the functional role of Thr74, the third site for phosphorylation that has been identified in *in vitro* studies. Unlike Ser281 and Thr444, phosphorylation of Thr74 appears not to have a direct role in stimulating catalytic activity but rather is crucial for binding S100B (*21*). It was therefore surprising to find that Thr74 is not located directly at the interface between NDR and S100B, and instead is exposed to solvent. This observation suggests that Thr74 could interact with another region of the catalytic domain and that its phosphorylation might serve as a switch for modulating the affinity between the two proteins.

Does the ability of dimeric S100B to bind two NDR molecules have any functional implications? While it is possible that steric factors preclude binding at a second S100B site, the dimer could function as a molecular bridge and influence the kinetics of autophosphorylation of Ser281 by an intermolecular mechanism. Alternatively, the second site could be involved primarily in recruiting a different kinase to phosphorylate Thr444 in the C-terminal domain (*21*). We are currently planning studies to test these hypotheses and further elucidate the mechanism of activation of the NDR kinase.

NOTE ADDED AFTER PRINT PUBLICATION

The name of author Brian A. Hemmings was incomplete in the version published on the Web 11/19/03 (ASAP) and in the December 16, 2003, issue (Vol. 42, No. 49, pp 14416−14426). The correct electronic version was published 01/12/06, and an Addition and Correction appears in the February 7, 2006, issue (Vol. 45, No. 5).

ACKNOWLEDGMENT

We thank Dr. Linda Van Eldik for providing the S100B gene, Dr. Haitao Hu for providing pulse sequences and useful advice on setting up NMR experiments, and Dr. Jarrod Smith for help in setting up AMBER calculations and for help with software-related queries.

SUPPORTING INFORMATION AVAILABLE

Model of the NDR kinase catalytic domain and sequence alignment of several members of the NDR family of kinases. This material is available free of charge via the Internet at http://pubs.acs.org.

REFERENCES

1. Zimmer, D. B., Cornwall, E. H., Landar, A., and Song, W. (1995) *Brain Res. Bull. 37*, 417−429.
2. Heizmann, C. W., and Cox, J. A. (1998) *Biometals 11*, 383−97.
3. Donato, R. (2001) *Int. J. Biochem. Cell Biol. 33*, 637−668.
4. Heizmann, C. W., Fritz, G., and Schäfer, B. W. (2002) *Frontiers Biosci. 7*, 1356−1368.
5. Mrak, R. E., Sheng, J. G., and Griffin, W. S. (1995) *Hum. Pathol. 26*, 816−823.
6. Castets, F., Griffin, W. S., Marks, A., and Van Eldik, L. J. (1997) *Brain Res. Mol. Brain Res. 46*, 208−16.
7. Heizmann, C. W. (1999) *Neurochem. Res. 24*, 1097−100.
8. Ikura, M., Osawa, M., and Ames, J. B. (2002) *Bioessays 24*, 625−636.
9. Huttunen, H. J., Kuja-Panula, J., Sorci, G., Agneletti, A. L., Donato, R., and Rauvala, H. (2000) *J. Biol. Chem. 275*, 40096−40105.
10. Schmidt, A. M., Yan, S. D., Yan, S. F., and Stern, D. M. (2001) *J. Clin. Invest. 108*, 949−955.
11. Bucciarelli, L. G., Wendt, T., Rong, L., Lalla, E., Hofmann, M. A., Goova, M. T., Taguchi, A., Yan, S. F., Yan, S. D., and Stern, D. M. (2002) *Cell. Mol. Life Sci. 59*, 1117−1128.
12. Millward, T., Cron, P., and Hemmings, B. A. (1995) *Proc. Natl. Acad. Sci. U.S.A. 92*, 5022−6.
13. Millward, T. A., Heizmann, C. W., Schäfer, B. W., and Hemmings, B. A. (1998) *EMBO J. 17*, 5913−22.
14. Selinfreund, R. H., Barger, S. W., Welsh, M. J., and Van Eldik, L. J. (1990) *J. Cell Biol. 111*, 2021−2028.
15. Geng, W., He, B., Wang, M., and Adler, P. N. (2000) *Genetics 156*, 1817−28.
16. Zallen, J. A., Peckol, E. L., Tobin, D. M., and Bargmann, C. I. (2000) *Mol. Biol. Cell 11*, 3177−90.
17. Verde, F., Wiley, D. J., and Nurse, P. (1998) *Proc. Natl. Acad. Sci. U.S.A. 95*, 7526−7531.
18. Bidlingmaier, S., Weiss, E. L., Seidel, C., Drubin, D. G., and Snyder, M. (2001) *Mol. Cell. Biol. 21*, 2449−62.
19. Hanks, S. K., and Hunter, T. (1995) *FASEB J. 9*, 576−596.
20. Millward, T. A., Hess, D., and Hemmings, B. A. (1999) *J. Biol. Chem. 274*, 33847−50.
21. Tamaskovic, R., Bichsel, S. J., Rogniaux, H., Stegert, M. R., and Hemmings, B. A. (2003) *J. Biol. Chem. 278*, 6710−6718.
22. Wilmann, M., Gautel, M., and Mayans, O. (2000) *Cell. Mol. Biol. 46*, 883−894.
23. Fritz, G., and Heizmann, C. W. (2003) *3D-Structures of the calcium and zinc binding S100 proteins*, Vol. 3, John Wiley & Sons, Chichester, New York, Weinheim, Brisbane, Singapore, Toronto.
24. Drohat, A. C., Amburgey, J. C., Abildgaard, F., Starich, M. R., Baldisseri, D., and Weber, D. J. (1996) *Biochemistry 35*, 11577−88.
25. Kilby, P. M., Van Eldik, L. J., and Roberts, G. C. (1996) *Structure 4*, 1041−52.
26. Drohat, A. C., Baldisseri, D. M., Rustandi, R. R., and Weber, D. J. (1998) *Biochemistry 37*, 2729−40.
27. Matsumura, H., Shiba, T., Inoue, T., Harada, S., and Kai, Y. (1998) *Structure 6*, 233−41.
28. Smith, S. P., and Shaw, G. S. (1998) *Structure 6*, 211−22.
29. Rety, S., Osterloh, D., Arie, J. P., Tabaries, S., Seeman, J., Russo-Marie, F., Gerke, V., and Lewit-Bentley, A. (2000) *Struct. Fold. Des. 8*, 175−84.
30. Van Eldik, L. J., Staecker, J. L., and Winningham-Major, F. (1988) *J. Biol. Chem. 263*, 7830−7837.
31. Wingfield, P. T., Palmer, I., Liang, S.-M., and Pain, R. H. (2002) in *Current Protocols in Protein Science* (Coligan, J. E., Dunn, B. M., Speicher, D. W., and Wingfield, P. T., Eds.) John Wiley and Sons, New York.
32. Muhandiram, D. R., and Kay, L. E. (1994) *J. Magn. Reson., Ser. B 103*, 203-216.
33. Cavanagh, J., Fairbrother, W. J., Palmer, A. G. I., and Skelton, N. J. (1996). *Protein NMR spectroscopy: Principles and practice*, Academic Press, San Diego.
34. Sattler, M., Schleucher, J., and Greisinger, C. (1999) *Prog. NMR Spectrosc. 34*, 93−158.
35. Kay, L. E., Xu, G. Y., Singer, A. U., Muhandiram, D. R., and Forman-Kay, J. D. (1993) *J. Magn. Reson., B 101*, 333−337.
36. Muhandiram, D. R., Farrow, N. A., Xu, G. Y., Smallcombe, S. H., and Kay, L. E. (1993) *J. Magn. Reson., B 102*, 317−321.
37. Talluri, S., and Wagner, G. (1996) *J. Magn. Reson., B 112*, 200−205.
38. Mori, S., Abeygunawardana, C., Johnson, M. O., and van Zijli, P. C. (1995) *J. Magn. Reson., B 108*, 94−98.
39. Rustandi, R. R., Baldisseri, D. M., and Weber, D. J. (2000) *Nat. Struct. Biol. 7*, 570−4.
40. Inman, K. G., Yang, R., Rustandi, R. R., Miller, K. E., Baldisseri, D. M., and Weber, D. J. (2002) *J. Mol. Biol. 24*, 1003−1014.
41. McClintock, K. A., and Shaw, G. S. (2002) *J. Biol. Chem. 278*, 6251−6257.
42. Ikura, M., and Bax, A. (1992) *J. Am. Chem. Soc. 114*, 2433−2440.
43. Lee, W., Revington, M. J., Arrowsmith, C., and Kay, L. E. (1994) *FEBS Lett. 350*, 87−90.
44. Vuister, G. W., Kim, S.-J., Wu, C., and Bax, A. (1994) *J. Am. Chem. Soc. 116*, 9206−9210.

45. Zwahlen, C., Legault, P., Vincent, S. J. F., Greenbalt, J., Konrat, R., and Kay, L. E. (1997) *J. Am. Chem. Soc. 119*, 6711−6721.
46. Duggan, B. M., Legge, G. B., Dyson, H. J., and Wright, P. E. (2001) *J. Biomol. NMR 19*, 321−329.
47. Wüthrich, K., Billeter, M., and Braun, M. (1983) *J. Mol. Biol. 169*, 949−961.
48. Güntert, P., Braun, W., and Wüthrich, K. (1991) *J. Mol. Biol. 217*, 517−530.
49. Güntert, P., Mumenthaler, C., and Wüthrich, K. (1997) *J. Mol. Biol. 273*, 283−298.
50. Cornilescu, G., Delaglio, F., and Bax, A. (1999) *J. Biomol. NMR 13*, 289−302.
51. Weiner, S. J., Kollman, P. A., Nguyen, D. T., and Case, D. A. (1986) *J. Comput. Chem. 7*, 230−252.
52. Pearlman, D. A., Case, D. A., Caldwell, J. C., Seibel, G. L., Singh, U. C., Weiner, P., and Kollman, P. A. (1991) *AMBER*, University of California.
53. Macke, T. J. (1996) Ph.D. Thesis, The Scripps Research Institute, La Jolla, CA.
54. Sastry, M., Ketchem, R. R., Crescenzi, O., Weber, C., Lubienski, M. J., Hidaka, H., and Chazin, W. J. (1998) *Structure 6*, 223−31.
55. Mäler, L., Potts, B. C., and Chazin, W. J. (1999) *J. Biomol. NMR 13*, 233−47.
56. Smith, J., Paloma, L. G., Case, D. A., and Chazin, W., J. (1996) *Magn. Reson. Chem. 34*, 147−155.
57. Laskowski, R. A., Rullman, J. A. C., MacArthur, M. W., Kaptein, R., and Thornton, J. M. (1996) *J. Biomol. NMR 8*, 477−486.
58. Koradi, R., Billeter, M., and Wüthrich, K. (1996) *J. Mol. Graphics 14*, 51−55.
59. Rety, S., Sopkova, J., Renouard, M., Osterloh, D., Gerke, V., Tabaries, S., Russo-Marie, F., and Lewit-Bentley, A. (1999) *Nat. Struct. Biol. 6*, 89−95.
60. McClintock, K. A., Van Eldik, L. J., and Shaw, G. S. (2002) *Biochemistry 41*, 5421−5428.
61. Landar, A., Rustandi, R. R., Weber, D. J., and Zimmer, D. B. (1998) *Biochemistry 37*, 17429−17438.
62. Garbuglia, M., Verzini, M., Rustandi, R. R., Osterloh, D., Weber, D. J., Gerke, V., and Donato, R. (1999) *Biochem. Biophys. Res. Commun. 254*, 36−41.
63. Seeman, J., Weber, K., and Gerke, V. (1996) *Biochem. J. 319*, 123−129.
64. Sopalla, C., Leukert, N., Sorg, C., and Kerkhoff, C. (2002) *Biol. Chem. 383*, 1895−1905.
65. Christakos, S., Gabrielides, C., and Rhoten, W. B. (1989) *Endocr. Rev. 10*, 3−26.
66. Ivanenkov, V. V., Jamieson, G. A., Gruenstein, E., and Dimlich, R. V. W. (1995) *J. Biol. Chem. 270*, 14651−14658.
67. McClintock, K. A., and Shaw, G. S. (2000) *Protein Sci. 9*, 2043−2046.
68. Brokx, R. D., Lopez, M. M., Vogel, H. J., and Makhatadze, G. I. (2001) *J. Biol. Chem. 276*, 14083−14091.
69. Rustandi, R. R., Baldisseri, D. M., Drohat, A. C., and Weber, D. J. (1999) *Protein Sci. 8*, 1743−51.
70. Peersen, O. B., Madsen, T. S., and Falke, J. J. (1997) *Protein Sci. 6*, 794−807.
71. Rustandi, R. R., Drohat, A. C., Baldisseri, D. M., Wilder, P. T., and Weber, D. J. (1998) *Biochemistry 37*, 1951−60.
72. Heierhorst, J., Kobe, B., Feil, S. C., Parker, M. W., Benian, G. M., Weiss, K. R., and Kemp, B. E. (1996) *Nature 380*, 636−9.
73. Heierhorst, J., Mann, R. J., and Kemp, B. E. (1997) *Eur. J. Biochem. 249*, 127−133.
74. Goldberg, J., Nairn, A. C., and Kuriyan, J. (1996) *Cell 84*, 857−887.
75. Huse, M., and Kuriyan, J. (2002) *Cell 109*, 275−282.
76. Thompson, J. D., Gibson, T. J., Plewniak, F., Jeanmougin, F., and Higgins, D. J. (1997) *Nucleic Acids Res. 24*, 4876−4882.
77. Sali, A., and Blundell, T. L. (1993) *J. Mol. Biol. 234*, 779−815.
78. Knighton, D. R., Zheng, J. H., Ten Eyck, L. F., Xuong, N. H., Taylor, S. S., and Sowadski, J. M. (1991) *Science 253*, 414−420.
79. Knighton, D. R., Zheng, J. H., Ten Eyck, L. F., Ashford, V. A., Xuong, N. H., Taylor, S. S., and Sowadski, J. M. (1991) *Science 253*, 407−414.
80. Bossemeyer, D., Engh, R. A., Kinzel, V., Ponstingl, H., and Huber, R. (1993) *EMBO J. 12*, 849−859.
81. Yang, J., Cron, P., Good, V. M., Thompson, V., Hemmings, B. A., and Barford, D. (2002) *Nat. Struct. Biol. 9*, 940−944.
82. Wybenga-Groot, L. E., Baskin, B., Ong, S. H., Tong, J., Pawson, T., and Sicheri, F. (2001). *Cell 106*, 745−757.

BI035089A